

Simulation of Steatosis Zonation in Liver Lobule—A Continuummechanical Bi-Scale, Tri-Phasic, Multi-Component Approach

Tim Ricken, Navina Waschinsky and Daniel Werner

Abstract The human liver is an important metabolic organ which regulates metabolism of the body in a complex time depending and non-linear coupled function-perfusion-mechanism. Harmful microstructure failure strongly affects the viability of the organ. The excessive accumulation of fat in the liver tissue, known as a fatty liver, is one of the most common liver micro structure failures, especially in western countries. The growing fat has a high impact on the blood perfusion and thus on the functionality of the organ. This interaction between perfusion, growth of fat and functionality on the hepatic microcirculation is poorly understood and many biological aspects of the liver are still subject of discussion. The presented computational model consists of a bi-scale, tri-phasic, multi-component approach based on the theory of porous media. The model includes the stress and strain state of the liver tissue, the transverse isotropic blood perfusion in the sinusoidal micro perfusion system. Furthermore, we describe the glucose metabolism in a two-scale PDE-ODE approach whereas the fat metabolism is included via phenomenological functions. Different inflow boundary conditions are tested against the influence on fat deposition and zonation in the liver lobules. With this example we can discuss biological assumptions and get a better understanding of the coupled function-perfusion ability of the liver.

1 Introduction

For a realistic simulation of the liver behavior it is important to take into account a detailed description of the biological processes. We present a bi-scale, tri-phasic, continuum multi-component model simulating blood perfusion and metabolism in

T. Ricken (✉) · N. Waschinsky · D. Werner
TU Dortmund, August-Schmidt-Straße 6, Dortmund, Germany
e-mail: tim.ricken@tu-dortmund.de

N. Waschinsky
e-mail: navina.waschinsky@tu-dortmund.de

D. Werner
e-mail: danielq.werner@tu-dortmund.de

© Springer International Publishing AG 2018
P. Wriggers and T. Lenarz (eds.), *Biomedical Technology*, Lecture Notes in Applied and Computational Mechanics 84, DOI 10.1007/978-3-319-59548-1_2

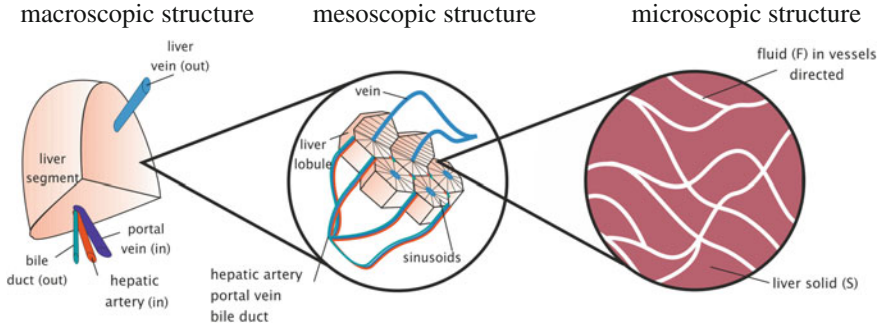


Fig. 1 Bi-scale approach; macroscopic structure: millimeter spatial resolution to observe the vascular system from the in- and outflow of the liver to smaller and smaller branches of the vessels; mesoscopic structure: micrometer spatial resolution to observe the perfusion through the sinusoids; microscopic structure: biochemical description of the metabolism in the liver cells

the human liver based on the two-phasic approach, see Ricken et al. [13]. To get a better understanding of the liver we start with a short physiological outline. For more informations, see Hubscher et al. [8].

The liver is the main metabolic organ in the human body. Roughly, the structure of the organ is segmented into four hepatic lobes of unequal size within the range of centimeters; the main parts are the right lobe (*lobus hepatic dexter*) and left lobe (*lobus hepatis sinister*). Each lobe consists of liver lobules which have the size of about a few millimeters. They are hexagonally structured parts of the liver tissue, see Fig. 1. Microscopic sized hepatocytes, the liver cells, are arranged in radial columns embedded in the liver lobules. The hepatic vascular system is important for the blood supply of the hepatocytes. For this, the vascular system consists of branches which supply the organ from the macroscopic to microscopic anatomy of the liver. On the macroscopic level branches of hepatic artery (oxygen rich) and portal vein (nutrient rich) run together and supply the segments of the organ. Intrahepatic bile ducts proceed together with the blood vessels and support the liver during detoxification processes as the bile fluid is excreted with decomposed products. The microcirculation takes place in the liver lobule. In each corner of the liver lobule a portal triad is located which is composed of the three branches of hepatic artery, portal vein and a bile duct in their smallest subdivision. The microcirculation is described by blood vessels connecting the portal triad with the central vein which are called sinusoids. The central vein drains the blood leading to a directed blood flow from the portal triad to the central vein, see Fig. 1.

Under consideration of the physiological background it is unavoidable to classify the liver in different scales to focus on scale depending processes.

We focus on a bi-scale approach; on the mesoscopic level we describe the blood perfusion through the liver lobule and on the microscopic level the metabolism in the cells.

The mesoscopic model is based on an ansatz for transverse isotropic permeability relation describing the perfusion given in Ricken et al. [12]. Due to the complex

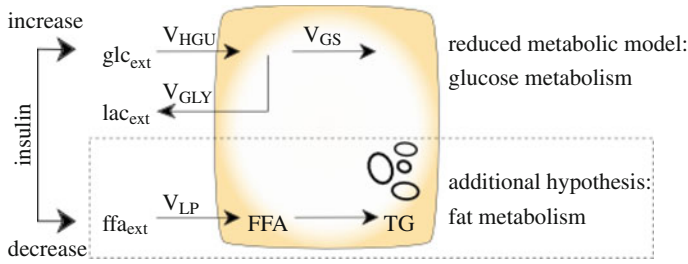


Fig. 2 Metabolism: the biochemical reactions are described with the metabolites of external glucose (glc_{ext}), external lactate (lac_{ext}), external FFA (ffa_{ext}), internal triglyceride (TG) and internal glycogen ($glyc$). External components are included in the fluid phase whereas internal components are included in the solid tissue of the liver. Triglyceride describes the fat phase in the liver. Reduced metabolic model: the glucose pathways (V_{HGU}), (V_{GS}) and (V_{GLY}) are modeled by sets of ordinary differential equations. With $V_{HGU} < 0$: hepatic glucose production, $V_{HGU} > 0$: hepatic glucose utilization, $V_{GLY} < 0$: gluconeogenesis, $V_{GLY} > 0$: glycolysis, $V_{GS} < 0$: glycogenolysis, $V_{GS} > 0$: glycogenesis. Additional hypothesis: the fatty acid pathway (V_{LP}) is modeled by assumptions concerning the uptake rate of FFA. With $V_{LP} > 0$: lipogenesis and $V_{LP} < 0$: lipolysis

vascular system of sinusoids it is impossible to model the numerous capillaries with an accurate discrete geometrical description. Therefore we apply a homogenized multiphase approach, based on the theory of porous media (TPM) which is a convenient tool in order to describe complex, multi-phasic and porous materials; see de Boer [2, 3] and Ehlers [5]. This approach includes the description of three main phases, namely the liver tissue, fat tissue and blood vessels. Additionally to the main phases, the homogenized liver lobule includes miscible components which are important for the biochemical description of the metabolism. A description of the mesoscopic model is given in the appendix.

We describe the biochemical processes on the microscopic scale of our model as the metabolism takes place in the smallest parts of the liver tissue, the cells. The liver is crucial for metabolites regulation of glucose and free fatty acid (FFA) due to its ability to store glucose in form of internal glycogen and FFA as internal fat deposition. The cells can switch between glucose and FFA deposition and utilization depending on the requirements of the rest of the body. After ingestions, glucose and FFA concentrations coming from the digestive system increase (hyperglycemia). The liver cells start to deposit them as internal metabolites glycogen and triglyceride. Whereas, during fasting times (hypoglycemia) the internal metabolites are served as a backup system and can be used to increase the low concentration of external metabolites. We summarize the metabolism in a set of ordinary differential equations which consider the conditions of hyperglycemia and hypoglycemia and the relations of the internal and external metabolites. The microscopic model approach is derived from a detailed pharmacokinetic model of hepatic glucose metabolism, described in König et al. [10]. We presented a reduced model for glucose metabolism in Ricken et al. [13] and add a phenomenological approach for the fat metabolism (Fig. 2).

2 Glucose and Fat Metabolism

The liver ensures biosynthetic metabolic pathways of immense complexity. In this study we focus on the main metabolic pathway of glucose described by a simplified ordinary differential equation system. Furthermore, we add a phenomenological approach for the fat metabolism.

Figure 2 summarizes the applied pathways for glucose and fat metabolism. The main task of the liver is the maintenance of homeostasis for metabolites which might be necessary for the organism. For this the liver regulates the glucose and fat level in order to offer enough energy for the brain and muscles. The metabolites are stored or utilized depending on hormone concentration levels. We distinguish two conditions: the fed (hyperglycemia) and fasted state (hypoglycemia). During feeding the organism is saturated of glucose and FFA leading to utilization of external metabolites. Glycolysis and glycogenesis are two possible metabolic pathways of glucose. The first metabolic pathway ensures the energy supply for cells and reproduction of lactate. The second describes energy storage in form of internal glycogen. Lipogenesis is the fatty acid pathway describing the ester of FFA and glycerol to triglyceride. The lipid accumulation is reinforced by high carbohydrate diets.

During the fasting state the organism utilizes hepatic glycogen, non-carbohydrate carbon substrates and lipids. Gluconeogenesis is one pathway for the generation of glucose. The utilization of certain non-carbohydrate carbon substrates provides a balanced glucose level. Breaking down hepatic glycogen describes the second mechanism to maintain glucose, namely glycogenolysis. The utilization of lipids is part of the lipolysis pathway and the reverse of lipogenesis. Molecules of lipids are hydrolyzed to glycerol and FFA.

For a realistic depiction of the liver functionalities, we take the above described main metabolic pathways into account. We use a reduced metabolic model, which has been derived from a detailed kinetic model of hepatic glucose metabolism, see König et al. [10]. It fully represents the metabolic behavior of depletion and utilization of glycogen. For further information see Ricken et al. [12, 13].

FFA play an important role in essential functions for the organism. They deliver cells energy and are important constituents for esterifying lipids. For a homeostatic circulation the organism can store, produce and consume FFA. This process is mainly regulated in the liver by fat metabolism. Stored triglyceride in adipocytes and dietary fat are sources, which ensure the availability of FFA in the liver. Beside the external concentration we need to take important enzymes and insulin into account. Insulin is a hormone which is distributed depending on the glucose concentration level in blood. The task of insulin is to regulate glucose and fat metabolism, so the pathways are coupled. Enzymes are responsible for hydrolysis of proteins, which bind FFA for circulation in the blood plasma.

The effects of fatty acid metabolism are not part of the kinetic model. In the following we present the assumptions concerning the FFA pathway. Equally to the glucose metabolism we calculate the rates of changing concentrations for the metabolites $\hat{p}^{\alpha\beta}$ contributing in the FFA pathway. We apply the influencing factors

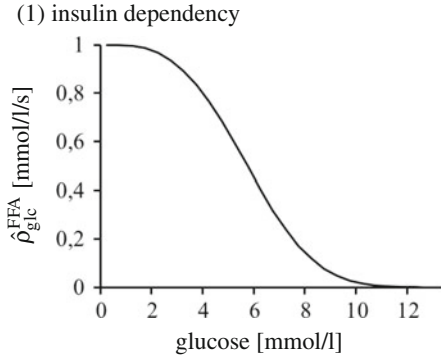


Fig. 3 Insulin dependency $\hat{\rho}_{glc}^{FFA}$: uptake rate of FFA depending on the concentration of glucose

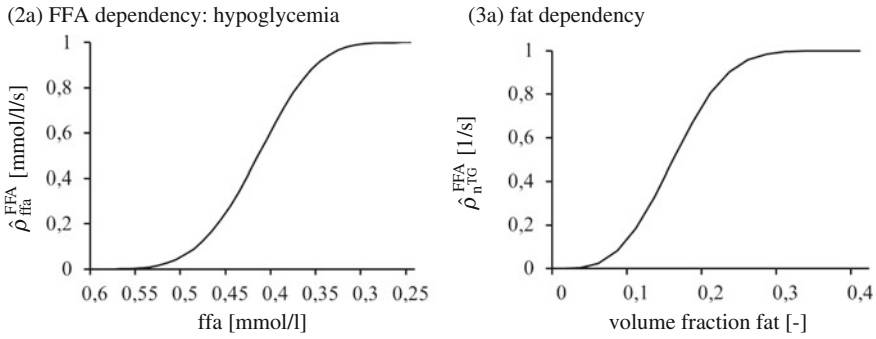


Fig. 4 Threshold of external FFA concentration 0, 6 mmol/l which leads to **a** hypoglycemic condition; **2a** FFA dependency $\hat{\rho}_{ffa}^{FFA}$: uptake rate of FFA depending on the external FFA concentration. **3a** fat dependency $\hat{\rho}_{nTG}^{FFA}$: uptake rate of FFA depending on the volume fraction of fat for a stable computation

$\left\{ \hat{\rho}_{glc}^{FFA}; \hat{\rho}_{ffa}^{FFA}; \hat{\rho}_{nL}^{FFA}; \hat{\rho}_{nTG}^{FFA} \right\}$. The terms are postulated via the differential equation of growth function with

$$\begin{aligned}
 \hat{\rho}_{glc}^{FFA} &= \exp^{-\log(2) \frac{glc^3}{glc_{Tp}^3}} \\
 \hat{\rho}_{ffa}^{FFA} &= +/ - 1 + \exp^{-40 * ((ffa - 0,6) * 2)^4} \\
 \hat{\rho}_{nL}^{FFA} &= -1 * \exp^{-\log(2) \frac{(a^L)^3}{0,15^3}} + 1 \\
 \hat{\rho}_{nTG}^{FFA} &= -1 * \exp^{-\log(2) \frac{(a^{TG})^3}{0,2^3}} + 1
 \end{aligned} \tag{1}$$

We calculate the maximum uptake rate of FFA considering insulin influence ($\hat{\rho}_{glc}^{FFA}$) which couples the glucose metabolism to the fat metabolism, see Fig. 3. Figure 4 summarizes the effects of hypoglycemic conditions which lead to

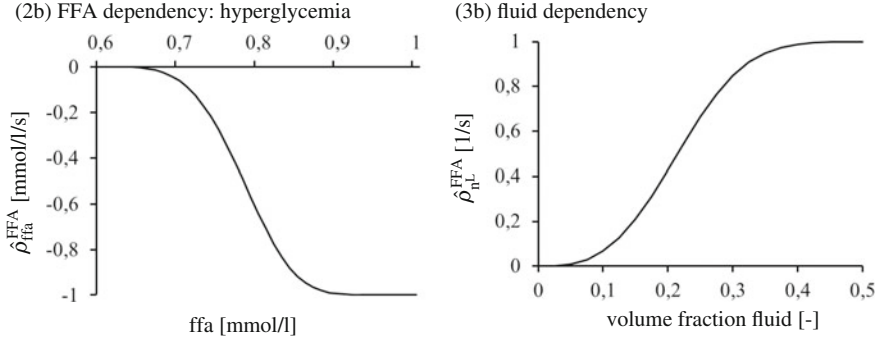


Fig. 5 Threshold of external FFA concentration 0, 6 mmol/l which leads to **b** hyperglycemic condition; **2b** FFA dependency $\hat{\rho}_{ffa}^{FFA}$: uptake rate of FFA depending on the external FFA concentration. **3b** fluid dependency $\hat{\rho}_{nl}^{FFA}$: uptake rate of FFA depending on the volume fraction of fluid for a stable computation

production of FFA. The uptake rate ($\hat{\rho}_{ffa}^{FFA}$) is positive as the organism needs more FFA for energy supply. The hypoglycemic condition results in phase transition from the fat phase to the fluid phase. To get a stable computation considering the saturation condition we take the influencing factor ($\hat{\rho}_{nTG}^{FFA}$) into account which steers an excessive increase of fluid. However, Fig. 5 shows the impact during hyperglycemic conditions. The uptake rate ($\hat{\rho}_{ffa}^{FFA}$) is negative as the liver stores redundant FFA and synthesizes lipids. In this case the fat phase gets additional mass and we steer an excessive increase of fat with ($\hat{\rho}_{nl}^{FFA}$).

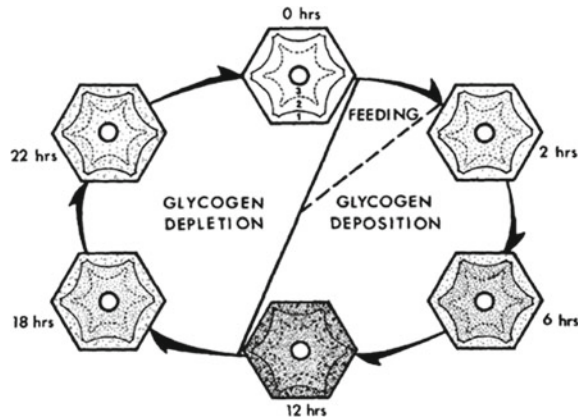
The mass exchange must fulfill the restrictions of the entropy inequality (24); the exchange can be summarized with

$$\bar{\psi}^{TG\beta} = \bar{\psi}^{TG} := \left[\hat{\rho}_{glc}^{FFA}, \hat{\rho}_{ffa}^{FFA}, \hat{\rho}_{nl}^{FFA}, \hat{\rho}_{nTG}^{FFA} \right]. \quad (2)$$

3 Numerical Example: Comparison of Different Assumptions for the Perfusion Coupled to the Metabolism

Many aspects of the liver are still subject of discussion. One example is the blood supplying system of the hepatic microcirculation. In this case it is still uncertain how the blood is emanating from the blood vessels into the liver lobule. One assumption, defined by Rappaport in 1954 [11], assumes an idealized hexagonal lobule which regards the portal triad as the ‘terminal portal venule’. This case regards the blood supplying system of the microcirculation initiated at the corners of the liver lobule, emanating from the portal triads. In a realistic framework, this point of view is not rational and a different assumption has to be applied. For this case

Fig. 6 Schematic sketch of the *feeding cycle* showing duration and typical patterns of glycogen in a single lobule during deposition and depletion. Figure reproduced from Babcock and Cardell [1]



Rappaport described additional portal venules which are derived from the portal vein and deliver the base of the liver lobule with inflowing blood. So the blood supplying system of the microcirculation is located at the surface of the liver lobule.

To get a better understanding of the different approaches and the influence on the metabolism, we simulate both hypotheses for the initial point of the microcirculation:

- Boundary-Model A: Idealized Case—Blood is emanating from the portal triad
- Boundary-Model B: Realistic Case—Blood is emanating from derived portal venules

In the numerical example we compute the microperfusion in one liver lobule coupled to the metabolism similar to Ricken et al. [13]. We evaluate the storage of internal glycogen deposition resulting from glucose metabolism analog to the experiments performed by Babcock and Cardell. In [1], Babcock and Cardell evaluated the glycogen storage during 24 h in one liver lobule after a feeding period (see Fig. 6). Furthermore we analyze the results of the fat metabolism which accrues in the hepatocytes (see Figs. 11–13).

We apply external boundary conditions for the glucose and FFA concentration which are applied in the feeding artery after one meal in 24 h (see Fig. 7). Furthermore we add external conditions for FFA. (cf. Stanhope et al. and Yuen et al. [14, 16])

The boundary conditions focus on the two different assumptions (see Fig. 8) for the initial point of the microcirculation (see Fig. 9). Additionally to the time depending DIRICHLET boundary conditions for the external concentration glucose and FFA, which depend on the food intake (see Fig. 7), we apply constant DIRICHLET boundary conditions for lactate at the inflow. As the blood flow is orientated in the direction of the pressure gradient (transverse isotropic permeability relation, Ricken et al. [13]) we apply a pressure difference between the inflow and the outflow with constant values (see Fig. 10).

Fig. 7 External boundary conditions: glucose profile corresponding to 2 h food intake and 22 h fasting based on 24 h profiles of plasma glucose (*red*). Analog profile for plasma FFA (*blue*). Experimental data from Stanhope et al. [14] and Yuen et al. [16]. Evaluation for numerical example after 6, 9 and 18 h

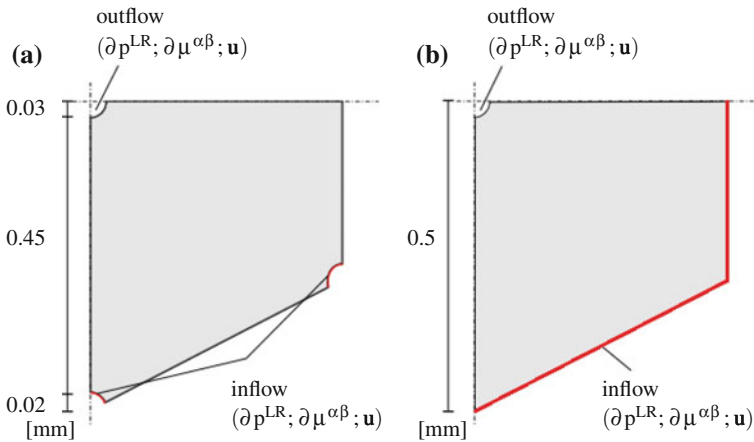
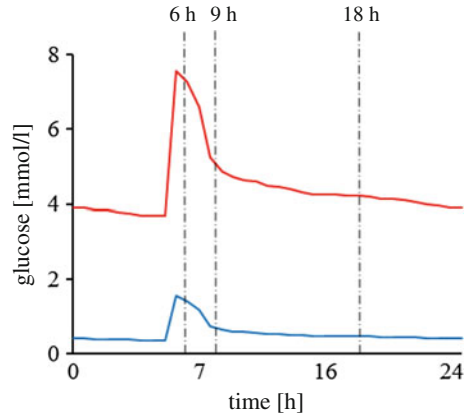


Fig. 8 Depiction of the applied geometry and boundary conditions. **a** Boundary-Model A **b** Boundary-Model B

3.1 Discussion

The simulation provides the evaluation of metabolites (see Figs. 11, 12, 13) resulting from glucose and fat metabolism. On the one hand we focused on the glucose pathway which depends on the external condition of blood glucose concentration. During hyperglycemic conditions the external concentration is high resulting in storage of glycogen. Whereas, a low glucose concentration encourages glycogen depletion. On the other hand we evaluated the phenomenological approach of the fat metabolism which leads to accumulation of fat depending on external blood FFA concentration. Based on the assumption that fat metabolism is inhibited by the presence of insulin we can observe the coupling between glucose and fat metabolism.

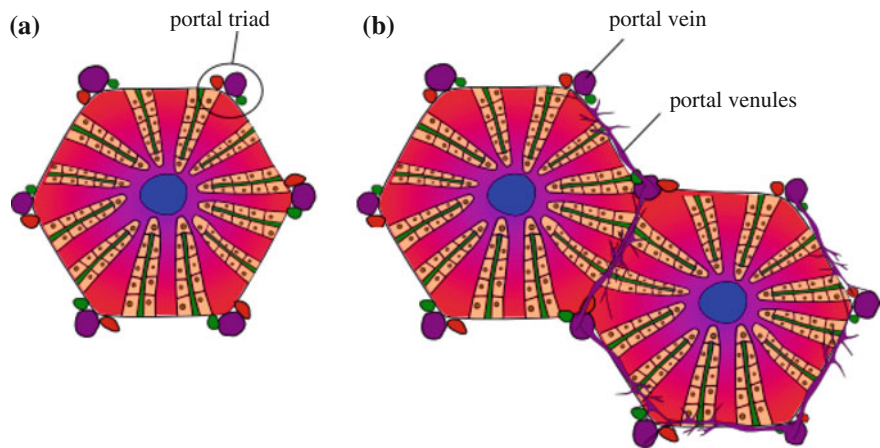


Fig. 9 Different assumptions for the blood supplying system of the microscopic circulation. **a** Boundary-Model A **b** Boundary-Model B

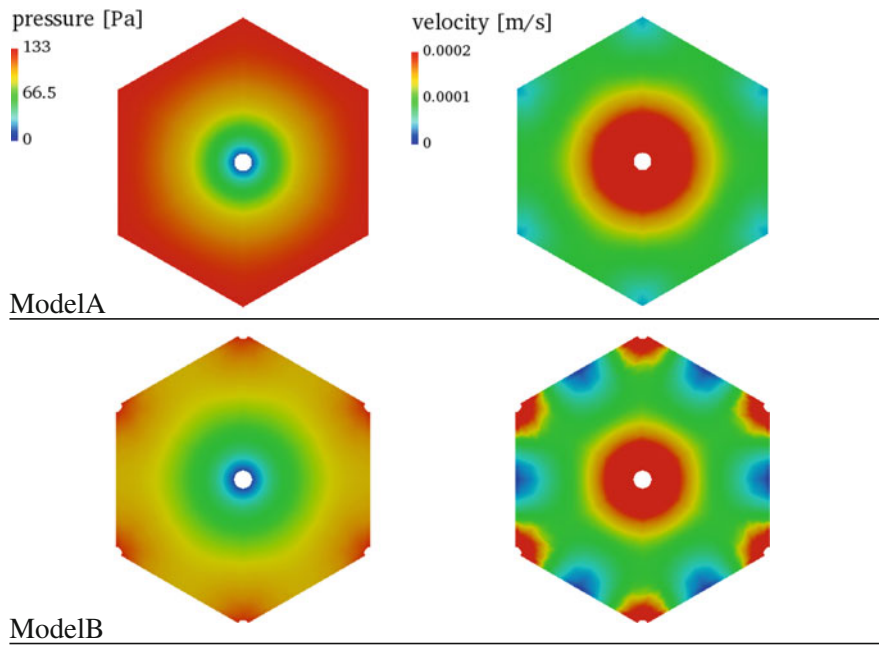


Fig. 10 Contour plot for the pressure distribution on the *left hand side* and velocity distribution on the *right hand side*. Comparison of the two assumptions for the boundaries; Boundary-Model A at top and Boundary-Model B beneath

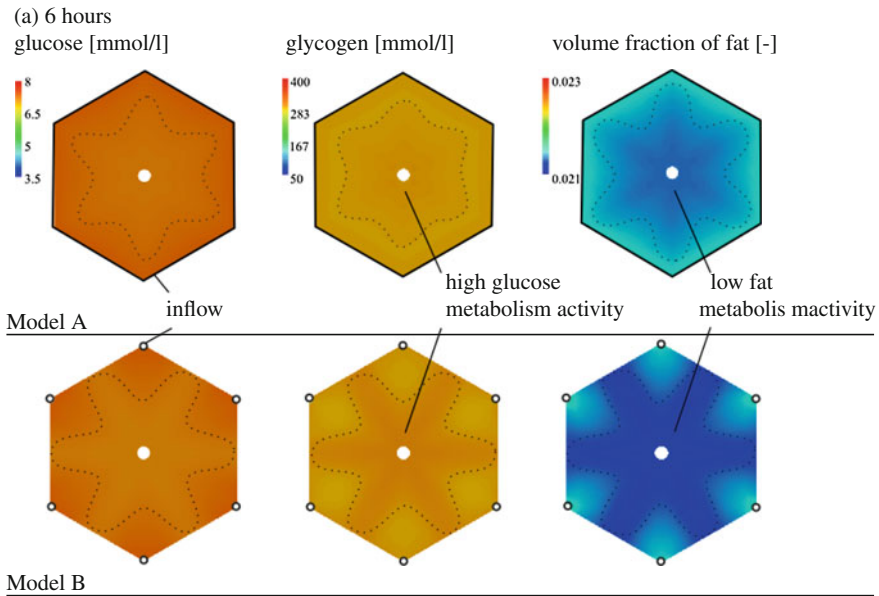


Fig. 11 Contour plot for the partial distribution after 6 h. Comparison of the two assumptions for the boundaries; Boundary-Model A at top and Boundary-Model B beneath

The main objective of this example is the comparison of the different boundary conditions as shown in Fig. 9. Figure 10 shows the influence on the microcirculation which results in a different velocity and pressure distribution. In the first case we assume idealized boundary conditions with an inflow emanating from the portal triad leading to a high pressure at the corners of the lobule. Based on the local pressure-modulated remodeling approach we get a directed blood flow depending on the gradient from the portal triad to the central vein. The velocity in between the portal triads is almost zero. The second assumption results in a high pressure on the lobule surface. The blood flow is directed from the surface to the center of the lobule with continuous values on the surrounding. The superposition at the portal triad leads to increased velocity. In conclusion the patterns of velocity are slightly twisted (see Fig. 10).

The Figs. 11, 12 and 13 evaluate the distribution of external concentration glucose, the deposition of glycogen and volume fraction of fat after 6, 9 and 18 h. The metabolism depends on the availability of metabolites in the lobule. As the motion of the external concentration is controlled by the blood flow, we can observe a higher activity of the glucose metabolism in areas with reduced velocity (more availability of metabolites). Hence, the different boundary conditions lead to slightly reversed depositions of glycogen in the lobule analogue to the microcirculation. The results of the experimental evaluation of the glycogen patterns in Fig. 6 are similar to the

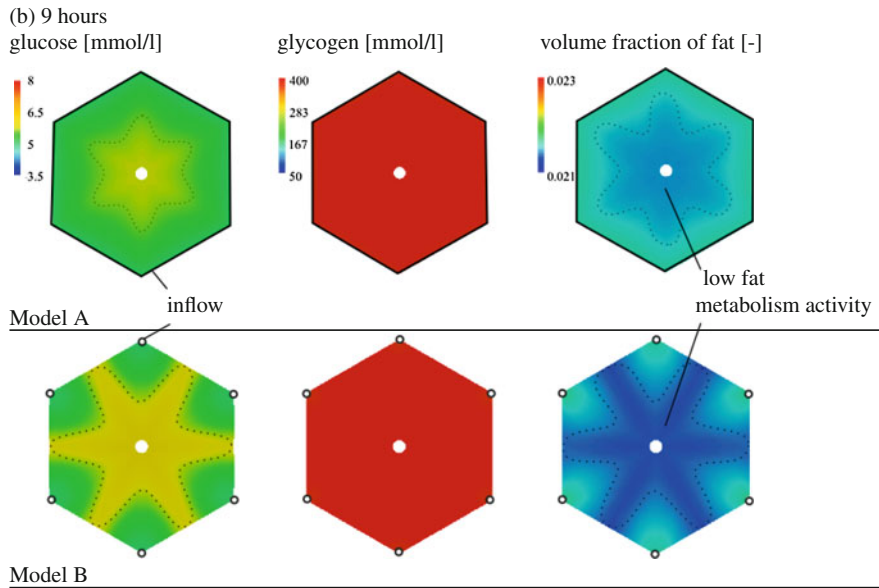


Fig. 12 Contour plot for the partial distribution after 9 h. Comparison of the two assumptions for the boundaries; Boundary-Model A at top and Boundary-Model B beneath

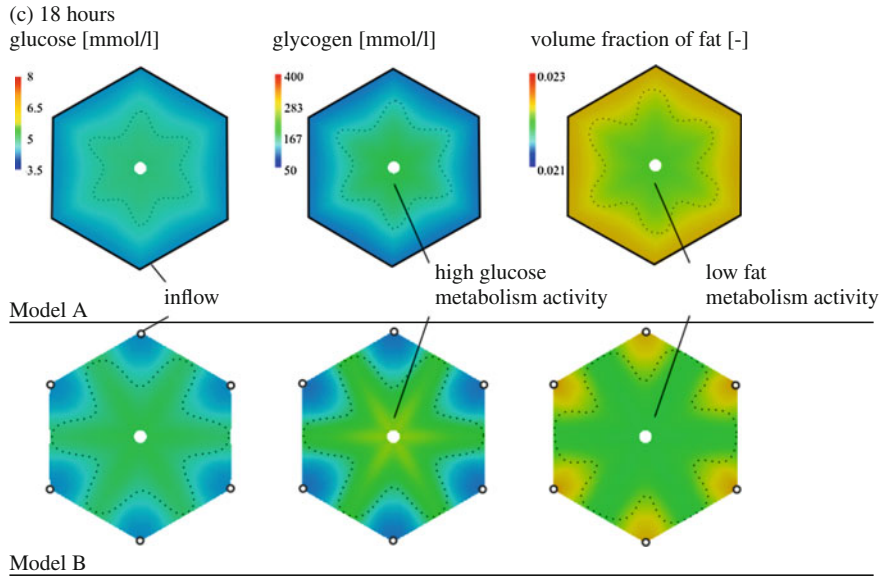


Fig. 13 Contour plot for the partial distribution after 18 h. Comparison of the two assumptions for the boundaries; Boundary-Model A at top and Boundary-Model B beneath

simulation with the boundary-model B and correlate to the hypothesis that additional venules support the microcirculation.

The development of the volume fraction of fat depends on the one hand on the availability of FFA and on the other hand it is controlled by insulin. In conclusion, a high activity of glucose metabolism leads to the release of insulin and the decrease of fat synthesis. Both models result in a higher concentration of lipids at the inflow area, the so called periportal zone of the liver lobule. This outcome is reasonable following the statement of Hubscher et al. who say that the “hepatocytes in the periportal zone have a higher capacity for [...] fatty acid metabolism” (Chap. 1, page 12 [8]).

Although the simulation focuses only on the quantitative evaluation, it approximates the patterns of metabolites in good accordance. Furthermore we could demonstrate that the metabolism including the phenomenological fat metabolism can be modeled via a bi-scale, tri-phasic approach. In this extended example (cf. Ricken et al. [13]) we show the influence of different boundary conditions and the importance of the biological background. But further investigations are needed to validate the fat metabolism and enlarge the applicability of the model to liver disease with growing fat influencing the metabolism.

Appendix

Perfusion-Model with a Multi-phasic Approach

The perfusion of the blood through the liver lobules is an important part to depict realistic descriptions for the viability of the organ. For that we use a homogenized approach on the mesoscopic scale, see Fig. 14. We consider three phases: the liver tissue φ^S , fat tissue φ^{TG} and fluid phase φ^L .

The phases are assumed as mutually immiscible materials φ^α with a heterogeneous arrangement in the overall volume. Each phase consists of a carrier phase φ^α , namely a solvent, and small miscible microscopic components $\varphi^{\alpha\beta}$, called solutes in the solvent. The TPM is an approach, which is composed of the mixture theory (Greve [7] and Hutter et al. [9]) and the concept of volume fractions (de Boer [2, 3] and Ehlers [5]). The saturation condition completes the approach.

The overall structure is a mixture of all included components, so the whole body φ can be decomposed by

$$\varphi = \sum_{\alpha=1}^{\kappa} \varphi^\alpha := \sum_{\alpha=1}^{\kappa} \left[\sum_{\beta=1}^{v-1} (\varphi^{\alpha\beta}) + \varphi^\alpha \right]. \quad (3)$$

To account the contribution of different phases we use the volume fraction n^α expressed by the ratio of partial volume dv^α to the overall mixture volume dv

$$n^\alpha = \frac{dv^\alpha}{dv}. \quad (4)$$

In view of the volume fractions, the saturations condition has to be fulfilled with

$$\sum_{\alpha=1}^{\kappa} n^\alpha \text{ mit } \kappa \in \{\mathbf{S}, \mathbf{TG}, \mathbf{L}\}. \quad (5)$$

For an effective connection between the mixture theory and the concept of volume fractions we consider the density ρ^α with

$$m = \sum_{\alpha=1}^{\kappa} m^\alpha = \int_{B_s} \sum_{\alpha=1}^{\kappa} \rho^\alpha dv. \quad (6)$$

where m is the mass of the mixture and m^α is the partial mass. Thereby ρ^α describes the partial density, which is derived by the ratio of mass dm^α to the volume dv of the structure

$$\rho^\alpha = \frac{dm^\alpha}{dv}. \quad (7)$$

The true density $\rho^{\alpha R}$ of the phases follows with

$$\rho^{\alpha R} = \frac{dm^\alpha}{dv^\alpha}. \quad (8)$$

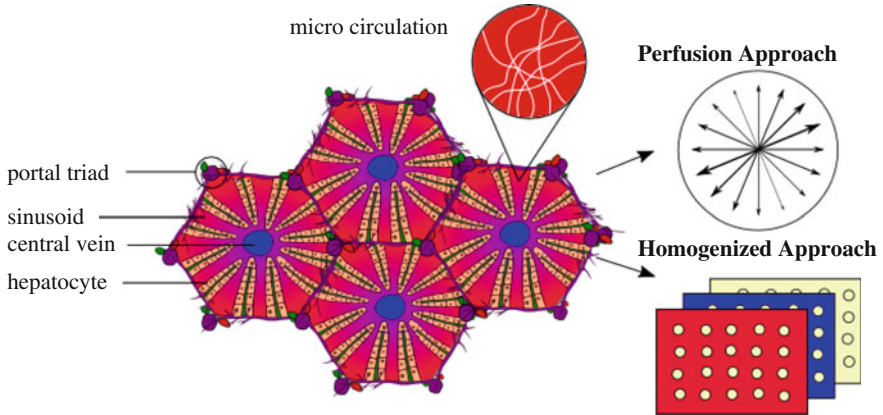


Fig. 14 Numerical implementation: perfusion approach with permeability in dependence of vessel distribution and preferred flow direction. Homogenization of the real structure into a smeared model (TPM)

Including the given Eqs. (3) and (8) we get a connection between the density and the volume fractions with

$$\rho^\alpha = \frac{dm^\alpha}{dv} = \frac{dm^\alpha}{dv^\alpha / n^\alpha} = n^\alpha \rho^{\alpha R}. \quad (9)$$

The concentration $c^{\alpha\beta}$ of the microscopic components which are included in the phases are described by the ratio of the number of moles dn_{mol}^β and the partial volume dv^α with

$$c^{\alpha\beta} = \frac{dn_{\text{mol}}^\beta}{dv^\alpha}. \quad (10)$$

The partial molar density of the microscopic components $\rho^{\alpha\beta}$ is decomposed by the volume fraction n^α , the concentration $c^{\alpha\beta}$ and the molecular weight M_{mol}^β of the constituent

$$\rho^{\alpha\beta} = n^\alpha c^{\alpha\beta} M_{\text{mol}}^\beta. \quad (11)$$

Whereas, the molecular weight of the constituent is calculated by the fraction of the mass dm^β of the component and the number of moles dn_{mol}^β

$$M_{\text{mol}}^\beta = \frac{dm^\beta}{dn_{\text{mol}}^\beta}. \quad (12)$$

Balance Equations in the Framework of TPM

The balance equations for the porous media contain the description for each phase φ^α analogous to a one phase continuum. The multiphase approach incorporates the chemical and physical interactions of the phases φ^α with the interaction forces $\hat{\mathbf{p}}^\alpha$ and the mass exchange $\hat{\rho}^\alpha$ following the metaphysical principles of Truesdell [15]. The local statements of the balance equation of mass, momentum and moment of momentum follow with

$$\begin{aligned} \sum_{\alpha=1}^{\kappa} \left[\frac{\partial n^\alpha}{\partial t} + \text{div}(n^\alpha \mathbf{x}'_\alpha) - \frac{1}{\rho^{\alpha R}} \hat{\rho}^\alpha \right] &= 0 \\ \sum_{\alpha=1}^{\kappa} [\text{div} \mathbf{T}^\alpha + \rho^\alpha (\mathbf{b}^\alpha - \mathbf{x}''_\alpha) + \hat{\mathbf{p}}^\alpha - \hat{\rho}^\alpha \mathbf{x}'_\alpha] &= \mathbf{0} \\ \sum_{\alpha=1}^{\kappa} [\mathbf{T}^\alpha - (\mathbf{T}^\alpha)^T] &= \mathbf{0} \end{aligned} \quad (13)$$

The balance equation of mass applies the time derivative ∂t of the volume fraction n^α . Furthermore, “div” describes the spatial divergence operator, \mathbf{x}'_α the velocity of the phases and $\rho^{\alpha R}$ the true density. \mathbf{T}^α is the Cauchy stress tensor, \mathbf{b}^α is the specific volume force and \mathbf{x}''_α describes acceleration. Truesdell introduced the metaphysical principles in [15] with fundamental formulations for the mixture bodies which lead to the restrictions

$$\begin{aligned} \sum_{\alpha=1}^{\kappa} \hat{\rho}^\alpha &= 0 \\ \sum_{\alpha=1}^{\kappa} \hat{\mathbf{p}}^\alpha &= \mathbf{0}. \end{aligned} \quad (14)$$

Assumptions for the Perfusion Model

In this approach we apply three main phases for the mixture body. Thus, the volume counts the main phases φ^α with $\alpha \in \mathbf{S}$ (liver tissue), \mathbf{TG} (fat tissue), \mathbf{L} (blood). We assume miscible concentrations included in the main phases which are important for the metabolism processes. The liver tissue is described by two components, the hepatocytes which include glycogen $\varphi^{S\beta} \in \{\text{Gy}\}$ as an internal concentration and fat as the second component which includes triglyceride $\varphi^{\text{TG}\beta} \in \{\text{TG}\}$. Both internal miscible components are results of the metabolism. Furthermore, the blood phase includes external solutes which are important metabolites coming from the intestines. Focusing on the glucose and fat metabolism we apply external concentrations for glucose, FFA and lactate $\varphi^{\text{L}\beta} \in \{\text{Gu}, \text{Lc}, \text{FFA}\}$. Since the overall solutes $\varphi^{\alpha\beta}$ are negligibly small in contrast to the phases φ^α we do not take the volume fraction of the concentrations into account. So, the volume of the main phases is nearly the same as the volume of the carrier phases and we can simplify $\varphi^\alpha \cong \varphi^\alpha$. Thus, we summarize the description for the mixture body with $\kappa = 3$

$$\varphi^\alpha = \{\text{S}, \text{TG}, \text{L}\} = \alpha_i \mid i = 1 \dots 3 \quad (15)$$

and $(\nu - 1)$ the microscopic components

$$\begin{aligned} \varphi^{S\beta} &= \{\text{Gy}\} &= \beta_i \mid i = 1 \\ \varphi^{\text{TG}\beta} &= \{\text{TG}\} &= \beta_i \mid i = 1 \\ \varphi^{\text{L}\beta} &= \{\text{Gu}, \text{Lc}, \text{FFA}\} &= \beta_i \mid i = 1 \dots 3 \end{aligned} \quad (16)$$

The overall volume v can be calculated by the volume fractions n^α of the phases

$$v = \sum_{\alpha=1}^{\kappa} dv^\alpha = \int_{\text{Bs}} \sum_{\alpha=1}^{\kappa} dv^\alpha = \int_{\text{Bs}} \sum_{\alpha=1}^{\kappa} n^\alpha dv \quad \text{mit} \quad \kappa \in \{\text{S}, \text{TG}, \text{L}\} \quad (17)$$

The basis of the TPM applies superimposed continua with interactions and independent motion functions for the included phases. De Boer [4] and Ehlers [5] give

an explanation of the kinematics of TPM. We assume a Lagrange description of the motion for the liver tissue $\chi_S(\mathbf{X}_S, t)$ with \mathbf{X}_S describing the reference configuration of the liver cells and t describing the time. As the fat tissue is connected to the liver cells we use the same motion function with $\chi_S = \chi_{TG}$. Additionally, the internal concentrations which are exclusively present in the cells of the liver have the same motion function as the liver and fat tissue. So we extend $\chi_S = \chi_{TG} = \chi_{S\beta} = \chi_{TG\beta}$. As a consequence of the identical motion function one velocity follows for the liver tissue, fat tissue and the internal concentration (glycogen, triglyceride) with $\mathbf{x}'_S = \mathbf{x}'_{TG} = \mathbf{x}'_{S\beta} = \mathbf{x}'_{TG\beta}$. Beside the fixed solid fraction the porous body contains the fluid phase which represents the blood flow. For the kinematics of the blood flow we use a modified Eulerian description with respect to the solid phase. We apply independent motion functions for the blood phase $\chi_L(\mathbf{X}_L, t)$ and the external concentration: glucose $\chi_{L,Gu}(\mathbf{X}_{L,Gu}, t)$, lactate $\chi_{L,Lc}(\mathbf{X}_{L,Lc}, t)$ and FFA $\chi_{L,FFA}(\mathbf{X}_{L,FFA}, t)$, which are included in the blood phase. The velocities follow with $\mathbf{x}'_L = \mathbf{x}'_L(\mathbf{X}_L, t)$ for the main phase of the fluid and $\mathbf{x}'_{L,Gu} = \mathbf{x}'_{L,Gu}(\mathbf{X}_{L,Gu}, t)$ for glucose, $\mathbf{x}'_{L,Lc} = \mathbf{x}'_{L,Lc}(\mathbf{X}_{L,Lc}, t)$ for lactate and $\mathbf{x}'_{L,FFA} = \mathbf{x}'_{L,FFA}(\mathbf{X}_{L,FFA}, t)$ for FFA.

The blood flow in the liver lobules mainly depends on the vascular system, which is designed by the sinusoidal arrangement. The sinusoids guide the blood from the portal triads to the central vein and lead to an anisotropic diffusivity. We introduced an approach for the anisotropic perfusion in Ricken et al. [13]. This includes an ansatz for the filter velocity $n^L \mathbf{w}_{LS}$ with the volume fraction of the fluid n^L and the seepage velocity \mathbf{w}_{LS} . The seepage velocity defines the difference in velocity of the fluid and solid phase $\mathbf{w}_{LS} = \mathbf{x}'_L - \mathbf{x}'_S$.

$$n^L \mathbf{w}_{LS} = k_{OS}^S \left(\frac{n^L}{1 - n_{OS}^S} \right)^m \mathbf{M}^* [-\text{grad} \lambda + \rho^{LR} \mathbf{b}] \quad (18)$$

It depends on the deformation $\left(\frac{n^L}{1 - n_{OS}^S} \right)^m$ (see Eipper [6]) which includes a dimensionless material parameter m , controlling the isotropic dependency of the permeability. Furthermore, it depends on the Darcy permeability with $k_{OS}^S \left[\frac{m^4}{Ns} \right]$ and on the transverse isotropic permeability relation \mathbf{M}^* which includes the alignment of the sinusoids (for further information see Ricken et al. [12, 13]).

Field Equations and Constitutive Modeling

Summarizing, we consider a quasi-static, isothermal, tri-phasic porous model with microscopic substances. The model takes into account an incompressible solid phase φ^S and fat phase φ^{TG} which are derived by the same motion function and an incompressible fluid phase φ^L . We assume mass exchange between the fat and fluid phase. All phases include substances $\varphi^{\alpha\beta}$ which are calculated by the microscopic model and allow phase transition to build up the metabolism. The solid phases φ^S and

fat phase φ^{TG} include the internal concentrations $\varphi^{S\beta}$ with $\varphi^{S\beta} \in \{\text{Gy}\}$ and $\varphi^{\text{TG}\beta}$ with $\varphi^{\text{TG}\beta} \in \{\text{TG}\}$. The external concentrations $\varphi^{L\beta}$ with $\varphi^{L\beta} \in \{\text{Gu}, \text{Lc}, \text{FFA}\}$ are included in the fluid phase. For the calculation of the presented model we use the following independent relations. On the one hand we use the local form of the balance equation of mass and momentum for each component with

$$\begin{aligned} (n^\alpha)'_\alpha + n^\alpha \operatorname{div} \mathbf{x}'_\alpha &= \frac{1}{\rho^{\alpha R}} \hat{\rho}^\alpha \\ \operatorname{div} \mathbf{T}^\alpha + \rho^\alpha \mathbf{b}^\alpha + \hat{\mathbf{p}}^\alpha &= \hat{\rho}^\alpha \mathbf{x}'_\alpha \end{aligned} \quad (19)$$

for the main phases and

$$\begin{aligned} (n^\alpha)'_{\alpha\beta} c^{\alpha\beta} M_{\text{mol}}^\beta + n^\alpha (c^{\alpha\beta})'_{\alpha\beta} M_{\text{mol}}^\beta + n^\alpha c^{\alpha\beta} M_{\text{mol}}^\beta \operatorname{div} \mathbf{x}'_{\alpha\beta} &= \hat{\rho}^{\alpha\beta} \\ \operatorname{div} \mathbf{T}^{\alpha\beta} + \rho^{\alpha\beta} \mathbf{b}^\alpha + \hat{\mathbf{p}}^{\alpha\beta} &= \hat{\rho}^{\alpha\beta} \mathbf{x}'_\alpha \end{aligned} \quad (20)$$

for the included concentrations. The field equations include the interaction terms between the main phases $\hat{\rho}^\alpha$ and the miscible substances $\hat{\rho}^{\alpha\beta}$. On the other hand we consider the physical constraint condition derived by the assumptions of the porous medium with the saturation condition

$$n^S + n^{\text{TG}} + n^L = 1, \quad (21)$$

the conditions for the mass exchange between the components with

$$\hat{\rho}^S + \hat{\rho}^{\text{TG}} + \hat{\rho}^L + \hat{\rho}^{\alpha\beta} = 0, \quad (22)$$

and the interaction forces

$$\hat{\mathbf{p}}^S + \hat{\mathbf{p}}^{\text{TG}} + \hat{\mathbf{p}}^L + \hat{\mathbf{p}}^{\alpha\beta} = \mathbf{0}. \quad (23)$$

Beside the field equations we need constitutive relations to complete the calculation concept of the saturated porous body. The constitutive equations are derived by the evaluation of the entropy inequality

$$\sum_{\alpha=1}^K [-\rho^\alpha (\psi^\alpha)'_\alpha - \hat{\rho}^\alpha (\psi^\alpha - \frac{1}{2} \mathbf{x}'_\alpha \cdot \mathbf{x}'_\alpha) + \mathbf{T}^\alpha \cdot \mathbf{D}_\alpha - \hat{\mathbf{p}}^\alpha \cdot \mathbf{x}'_\alpha] \geq 0, \quad (24)$$

The constitutive equations follow with

Table 1 Material parameters of liver lobule

Parameter	Value	Unit	Remark
n_{0S}^S	0.8	–	Volume fraction solid
n_{0S}^{TG}	0.02	–	Volume fraction fat
n_{0S}^L	0.18	–	Volume fraction fluid
μ^S, μ^{TG}	4×10^4	Pa	Lam constant
λ^S, λ^{TG}	3×10^4	Pa	Lam constant
θ	280	K	Temperature
R	8.3144	J/molK	Gas constant
k_D^L	4.5×10^{-10}	m/s	Darcy permeability

$$\begin{aligned}
\mathbf{T}^S + \mathbf{T}^{S\beta} + \mathbf{T}^{TG} + \mathbf{T}^{TG\beta} &= 2\rho^S \mathbf{F}_S \frac{\partial \psi^S}{\partial \mathbf{C}_S} \mathbf{F}_S^T + 2\rho^{TG} \mathbf{F}_S \frac{\partial \psi^{TG}}{\partial \mathbf{C}_S} \mathbf{F}_S^T \\
&\quad - (n^S + n^{TG}) \lambda \mathbf{I} \\
\mathbf{T}^L &= -\lambda n^L \mathbf{I} + \rho^{\alpha\beta} c^{\alpha\beta} \frac{\partial \psi^{\alpha\beta}}{\partial c^{\alpha\beta}} \mathbf{I} \\
\mathbf{T}^{L\beta} &= -\rho^{\alpha\beta} c^{L\beta} \frac{\partial \psi^{\alpha\beta}}{\partial c^{\alpha\beta}} \mathbf{I}.
\end{aligned} \tag{25}$$

for the description of the stresses.

We postulate a hyperelastic material description of the solid following the Hooke's law with the Neo-Hookean Helmholtz free energy function

$$\begin{aligned}
\psi^S &= \frac{1}{\rho_{0S}^S} \left[\lambda^S \frac{1}{2} (\ln J_S) - \mu^S \ln J_S + \frac{1}{2} \mu^S (\text{tr } \mathbf{C}_S - 3) \right] \\
\psi^{TG} &= \frac{1}{\rho_{0S}^{TG}} \left[\lambda^{TG} \frac{1}{2} (\ln J_S) - \mu^{TG} \ln J_S + \frac{1}{2} \mu^{TG} (\text{tr } \mathbf{C}_S - 3) \right]
\end{aligned} \tag{26}$$

including the Lamé constants λ^S and μ^S for the liver solid and λ^{TG} and μ^{TG} for the liver fat (Table 1). Moreover we describe the free energy function for the concentrations $\psi^{\alpha\beta}$ with the general gas constant $R [\frac{\text{J}}{\text{molK}}]$, the temperature of the mixture $\theta [\text{K}]$, the molecular weight of the constituent $M_{\text{mol}}^\beta [\frac{\text{g}}{\text{mol}}]$ and the reference chemical potential $\mu_0^{\alpha\beta} [\frac{\text{J}}{\text{mol}}]$

$$\psi^{\alpha\beta} = \frac{1}{c^{\alpha\beta}} \left[\frac{R \theta}{M_{\text{mol}}^\beta} \left(\ln \left(\frac{c^{\alpha\beta}}{c_0^{\alpha\beta}} \right) - 1 \right) + \mu_0^{\alpha\beta} \right]. \tag{27}$$

References

1. M.B. Babcock, R.R. Cardell, Hepatic glycogen patterns in fasted and fed rats. *Am. J. Anat.* **140**(3), 299–337 (1974)

2. R. Boer, *Theory of Porous Media: Highlights in Historical Development and Current State* (Springer, New York, 2000)
3. R. De Boer, Highlights in the historical development of the porous media theory: toward a consistent macroscopic theory. *Appl. Mech. Rev.* **49**(4), 201–262 (1996)
4. R. De Boer, *Theory of Porous Media: Highlights in Historical Development and Current State*, (Springer Science & Business Media, 2012)
5. W. Ehlers, *Foundations of Multiphase and Porous Materials*, (Springer, 2002)
6. G. Eipper, *Theorie und Numerik Finiter Elastischer Deformationen in Fluidgesättigten Porösen Festkörpern*. PhD thesis, Inst. für Mechanik, (Bauwesen, 1998)
7. R. Greve, *Kontinuumsmechanik: Ein Grundkurs für Ingenieure und Physiker*, (Springer, 2013)
8. S.G. Hubscher, A.D. Burt, B.C. Portmann, L.D. Ferrell, *MacSween's Pathology of the Liver*, (Elsevier Health Sciences, 2011)
9. K. Hutter, K. Jöhnk, *Continuum Methods of Physical Modeling: Continuum Mechanics, Dimensional Analysis, Turbulence*, (Springer Science & Business Media, 2013)
10. M. König, S. Bulik, H.-G. Holzhütter, Quantifying the contribution of the liver to glucose homeostasis: a detailed kinetic model of human hepatic glucose metabolism. *PLoS Comput. Biol.* **8**(6), e1002577 (2012)
11. A. Rappaport, Z. Borowy, W. Loughheed, W. Lotto, Subdivision of hexagonal liver lobules into a structural and functional unit. role in hepatic physiology and pathology. *Anat. Rec.* **119**(1), 11–33 (1954)
12. T. Ricken, U. Dahmen, O. Dirsch, A biphasic model for sinusoidal liver perfusion remodeling after outflow obstruction. *Biomech. Model. Mechanobiol.* **9**(4), 435–450 (2010)
13. T. Ricken, D. Werner, H. Holzhütter, M. König, U. Dahmen, O. Dirsch, Modeling function-perfusion behavior in liver lobules including tissue, blood, glucose, lactate and glycogen by use of a coupled two-scale pde-ode approach. *Biomech. Model. Mechanobiol.* **14**(3), 515–536 (2015)
14. K.L. Stanhope, S.C. Griffen, B.R. Bair, M.M. Swarbrick, N.L. Keim, P.J. Havel, Twenty-four-hour endocrine and metabolic profiles following consumption of high-fructose corn syrup-, sucrose-, fructose-, and glucose-sweetened beverages with meals. *Am. J. Clin. Nutr.* **87**(5), 1194–1203 (2008)
15. C. Truesdell, Thermodynamics of diffusion. In *Rational Thermodynamics*, (Springer, 1984), pp. 219–236
16. K.C. Yuen, P.A. McDaniel, M.C. Riddle, Twenty-four-hour profiles of plasma glucose, insulin, c-peptide and free fatty acid in subjects with varying degrees of glucose tolerance following short-term, medium-dose prednisone (20 mg/day) treatment: evidence for differing effects on insulin secretion and action. *Clin. Endocrinol.* **77**(2), 224–232 (2012)

Biomedical Technology

Modeling, Experiments and Simulation

Wriggers, P.; Lenarz, Th. (Eds.)

2018, IX, 362 p. 166 illus., 135 illus. in color., Hardcover

ISBN: 978-3-319-59547-4